Title

Structure of superhard tungsten tetraboride: A missing link between MB2 and MB12 higher borides

Journal

Proceedings of the National Academy of Sciences of the United States of America, 112(11)

ISSN

0027-8424

Authors

Lech, Andrew T
Turner, Christopher L
Mohammadi, Reza
et al.

Publication Date

2015-03-17

DOI

10.1073/pnas.1415018112

Peer reviewed

Structure of superhard tungsten tetraboride: A missing link between MB_2 and MB_{12} higher borides

Andrew T. Lech[a], Christopher L. Turner[a], Reza Mohammadi[b], Sarah H. Tolbert[a,c,d], and Richard B. Kaner[a,c,d,1]

[a]Department of Chemistry and Biochemistry, University of California, Los Angeles, CA 90095; [b]Department of Mechanical and Nuclear Engineering, Virginia Commonwealth University, Richmond, VA 23284; [c]Department of Materials Science and Engineering, University of California, Los Angeles, CA 90095; and [d]California NanoSystems Institute, University of California, Los Angeles, CA 90095

Edited by Zachary Fisk, University of California, Irvine, CA, and approved February 3, 2015 (received for review August 13, 2014)

Superhard metals are of interest as possible replacements with enhanced properties over the metal carbides commonly used in cutting, drilling, and wear-resistant tooling. Of the superhard metals, the highest boride of tungsten—often referred to as WB_4 and sometimes as $W_{1-x}B_3$—is one of the most promising candidates. The structure of this boride, however, has never been fully resolved, despite the fact that it was discovered in 1961—a fact that severely limits our understanding of its structure–property relationships and has generated increasing controversy in the literature. Here, we present a new crystallographic model of this compound based on refinement against time-of-flight neutron diffraction data. Contrary to previous X-ray–only structural refinements, there is strong evidence for the presence of interstitial arrangements of boron atoms and polyhedral bonding. The formation of these polyhedra—slightly distorted boron cuboctahedra—appears to be dependent upon the defective nature of the tungsten-deficient metal sublattice. This previously unidentified structure type has an intermediary relationship between MB_2 and MB_{12} type boride polymorphs. Manipulation of the fractionally occupied metal and boron sites may provide insight for the rational design of new superhard metals.

superhard | borides | tungsten tetraboride | neutron diffraction | Rietveld refinement

As demand increases for new superhard materials, the introduction of transition metal borides as candidate compounds has recently attracted a great deal of attention (1–4). This trend is at least partially driven by a need for greater efficiency in cutting tools compared with tungsten carbide (which is not superhard), as well as the shortcomings of the traditional superhard compounds—diamond (which is unusable for cutting ferrous materials) (5) and cubic boron nitride (which is very expensive to synthesize and difficult to shape) (6). Within the rapidly growing family of superhard borides, tungsten tetraboride (or WB_4) is of specific interest due to its excellent mechanical properties and its relatively lower cost compared with borides such as ReB_2, OsB_2, RuB_2, and RhB_2, which contain platinum group metals (3, 7–11). For instance, tungsten tetraboride demonstrates an extremely high indentation hardness of ~43 GPa by the Vickers method (under an applied load of 0.49 N) (8) and ~41.7 GPa by nanoindentation (maximum, at a penetration depth of 95.25 nm; Fig. 1), and can sustain a differential stress (a lower-bound estimate of compressive yield strength) of up to ~19.7 GPa (12). More dramatically, it is like ReB_2 (2), capable of scratching natural diamond (11). We have, furthermore, previously shown that the hardness of this compound may be enhanced by the creation of solid solutions with other transition metals (9). However, to understand the underlying mechanisms for the hardness enhancements observed in WB_4 solid solutions, as well as to guide the design of new superhard borides with tailored mechanical properties, it is crucial to understand the crystal structure of this compound.

Perhaps surprisingly for a simple binary compound, the structure of tungsten tetraboride has been a contentious issue since its discovery by Chretien and Helgorsky in 1961, who assumed it to be related to borides of the ThB_4 type (tetragonal, $a = 6.34$ Å and $c = 4.50$ Å) (13). Currently, no fewer than four distinct structures have been proposed for this compound (Table 1), the three most plausible of which are illustrated in Fig. 2. Because of the discrepancies among published structural models, the present study was undertaken with the goal of revisiting the structure of this boride using the additional resource of neutron diffraction, a technique that is complementary to X-ray diffraction. Thermal neutrons, interacting in this case entirely with atomic nuclei, have a very high scattering cross-section for boron-11. This situation is opposite from that in X-ray diffraction, where scattering is dictated by electron clouds, and is thus dominated by the considerably more electron-dense tungsten atoms.

Having simultaneously refined against data obtained from these two methods, we have produced what we believe to be the definitive structural model for the highest boride of tungsten. As a result, the structure reported here, which contains some elements already known from previous X-ray–only investigations, introduces several previously unidentified ones that are observable only with the more detailed information derived from neutron data. Most importantly, however, this model provides insight into the rational causes of the extremely high hardness and solid solution hardening behavior observed in this boride. The history of previous attempts has already been explored in the recent work of Zeiringer et al. (14), and therefore will be only briefly summarized here.

Arguably the most cited of the structural solutions for WB_4, and the first for which atomic coordinates were assigned, was produced by Romans and Krug (15) in 1965. This structure (Fig. 2*A*) was based on refinement of powder diffraction data against

Significance

Superhard materials are those with hardness competitive with diamond. This study investigates tungsten tetraboride, a superhard metallic compound, and a promising candidate to revolutionize cutting tools and to succeed the "hard metals," such as tungsten carbide, that are commonly used. Unfortunately, the structure of this material has been contested for over half a century. Previous attempts at its solution have lacked comprehensiveness, as they have not used techniques, such as neutron diffraction, which are capable of differentiating between light and heavy elements (boron and tungsten, respectively). Utilizing both X-ray and neutron diffraction, this study reveals that tungsten tetraboride is actually an interesting 'new' structural hybrid between lower and higher borides, a missing link that further confirms the structural regularity among borides.

Author contributions: A.T.L. and R.M. designed research; A.T.L. and C.L.T. performed research; A.T.L. analyzed data; and A.T.L., C.L.T., R.M., S.H.T., and R.B.K. wrote the paper.

The authors declare no conflict of interest.

This article is a PNAS Direct Submission.

[1]To whom correspondence should be addressed. Email: kaner@chem.ucla.edu.

This article contains supporting information online at www.pnas.org/lookup/suppl/doi:10.1073/pnas.1415018112/-/DCSupplemental.

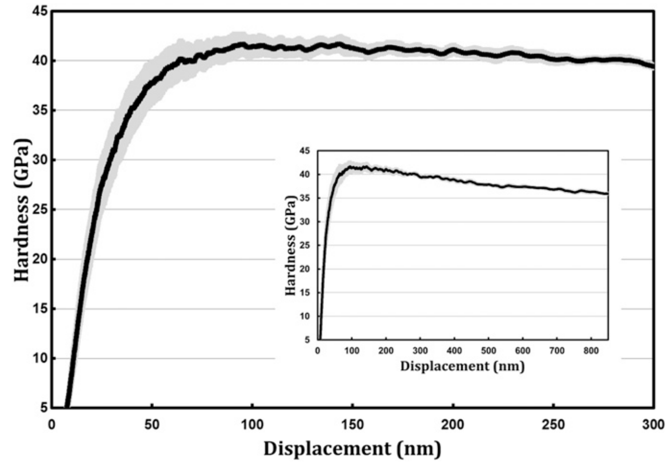

Fig. 1. Plot of average nanoindentation hardness versus displacement for WB_4, indicating superhardness (hardness above 40 GPa) from ∼60 nm displacement to ∼250 nm. The average hardness over this range is 40.9 ± 1.1 GPa with a maximum value of 41.7 ± 1.3 GPa at 95.25 nm. The shaded area represents the 95% confidence interval. (*Inset*) The full hardness curve from 0 to 850 nm. The average value of hardness from 60 to 850 nm is 39.7 ± 0.8 GPa. Numbers following the ± sign represent SDs.

a lower volume (148.47 vs. 180.88 $Å^3$) hexagonal unit cell (space group $P6_3/mmc$, $a = 5.200$ Å and $c = 6.340$ Å) versus the tetragonal assumption of Chretien and Helgorsky. After assigning the tungsten sites, having assumed them to be fully occupied, they accommodated their measured stoichiometry (WB_4 – WB_5) by designating Wyckoff positions *12(i)* and *4(f)* as boron sites. This assumption produced reasonable B—B bond lengths, but resulted in the imposition of B—B dimers, or "dumbbells" within the tungsten layers.

Independently, Nowotny et al. explored the system in 1967 using tungsten borides isolated from eutectic melts of MB—WB_4—B (M = Ni, Rh, Pd, Pt), and assigned the formula $W_{2-x}B_9$ to the highest boride (approximate composition $W_{1.83}B_9$ or $WB_{4.92}$). Perhaps due to indexing a few contaminating X-ray lines (discussed below), they assigned it to the low-symmetry trigonal group *P-3* with $a = 5.206$ Å and $c = 6.335$ Å (Fig. 2*B*) (16). Instead of dumbbells, their structure includes B_6 octahedra inserted among the ordered tungsten vacancy positions. The Nowotny et al. model is probably most notable for being the first to anticipate fractional occupancy at the tungsten *2*(*b*) site.

To settle the already clear incongruity of the above structures, Rosenberg and Lundström attempted a definitive solution for the positions of the boron atoms in 1973 using computerized least-squares refinement and Fourier difference map techniques (17). To minimize the scattering power mismatch between metal atoms and boron, they refined, as proxy, the presumably isomorphous molybdenum phase denoted $Mo_{1-x}B_3$ ($x \sim 0.20$) (Fig. 2*C*). Although this work confirmed the partial occupancy at one of the metal sites, the possibility of boron atoms filling vacancies in the structure was rejected, leaving voids in the structure. This model has been lent even more support by a recent single-crystal investigation by Zeiringer et al., who worked directly with the tungsten phase, referring to it analogously as $W_{1-x}B_3$ ($P6_3/mmc$, $a = 5.2012$ Å and $c = 6.3315$ Å) (14), seemingly settling the matter.

Outside the X-ray crystallographic community, however, this issue has also attracted significant attention from theoretical groups. Within the past five years, there has been a rapid succession of computational papers with the goal of identifying the structural origin of the properties of WB_4 (18–28). Although the correctness of the Romans and Krug model was initially assumed (24), it was quickly noticed that such a structure should be unstable (26). This lead to the theoretical confirmation that the structure and properties of the highest boride of tungsten are better accommodated if the B_2 dimers are removed (21, 23, 27), producing a composition of WB_3. Most recently, several exotic models have appeared with larger unit cells (18, 29) and varying stacking orders (28) of the metal layers. So far, all of these models still appear inconsistent with the experimental evidence. Thus, although nearly all current experimentally derived models agree that partial occupancy plays a role in the structure of WB_4, computational support is still weak (21). This situation may change as computing resources increase (enabling, for instance, much larger supercell models), but as it stands, the calculations so far reported only further highlight the structural ambiguity of this compound and do not themselves offer a viable alternative consistent with experiment.

Results and Discussion

The ambiguity in experimental determinations of the highest boride of tungsten stems primarily from difficulties in refining X-ray diffraction data for a compound containing closely associated elements that are near the extremes of being electron poor (boron; $Z = 5$) and electron rich (tungsten; $Z = 74$). Although the ratio of boron to tungsten is large, it is not so large that boron's core-electron contribution dominates the structure factor. This situation is exacerbated by three further issues: (*i*) the imprecision with which the compound's stoichiometry is known, (*ii*) the synthetic necessity to include excess boron to avoid WB_2 impurities; and (*iii*) partial occupancy at sites in the tungsten layer.

Fortunately, the disparity between the diffraction contributions of the two elements can be significantly decreased using thermal neutron diffraction, where the scattering power for both elements is roughly comparable. Thus, by simultaneous refinement of patterns obtained using both diffraction techniques, it becomes possible to distinguish between several possible atomic arrangements that all appear consistent with X-ray data alone. This approach is similar to the rationale used by Rosenberg and Lundström, whose modeling was based on an analogous compound, $Mo_{1-x}B_3$, where the lower atomic number of molybdenum was used to enhance the contribution of boron to the X-ray structure factor. Nevertheless, we believe the present method to be superior because we work with the native compound and therefore avoid assumptions about similarities between the W and Mo borides.

However, because we have found that the approximate eutectic composition W:B = 1:12 most reliably produces "WB_4" without additional tungsten-containing phases (8), our approach is still complicated by the presence of superstoichiometric amounts of boron. This excess boron crystallizes exclusively as the β-rhombohedral phase without crystallographically identifiable dissolution of tungsten (as found here and corroborated by ref. 30), and its

Table 1. Summary of previous WB_4 models

	Romans and Krug WB_4	Nowotny et al. $W_{2-x}B_9$	Zeiringer et al. $W_{1-x}B_3$	Theory WB_3
Formula	WB_4	$W_{1.83}B_{4.9}$	$W_{0.86}B_3$	WB_3
Space group	$P6_3/mmc$	*P -3*	$P6_3/mmc$	$P6_3/mmc$
a/Å = b/Å	5.200	5.206	5.2012	∼5.20
c/Å	6.34	6.335	6.3315	∼6.34
W1 occ. (site)	1 (*2c*)	1 (*2d*)	1 (*2c*)	1 (*2c*)
W2 occ. (site)	1 (*2b*)	∼0.833 (*2c*)	0.725 (*2b*)	1 (*2b*)
B1 occ. (site)	1 (*12i*)	1 (*6g*)	1 (*12i*)	1 (*12i*)
B2 occ. (site)	1 (*4f*)	1 (*6g*)	—	—
B3	—	1 (*6g*)	—	—
Notes	B_2 dimers	Frac. Occ., B_6 octahedra	Frac. Occ., voids	Idealized

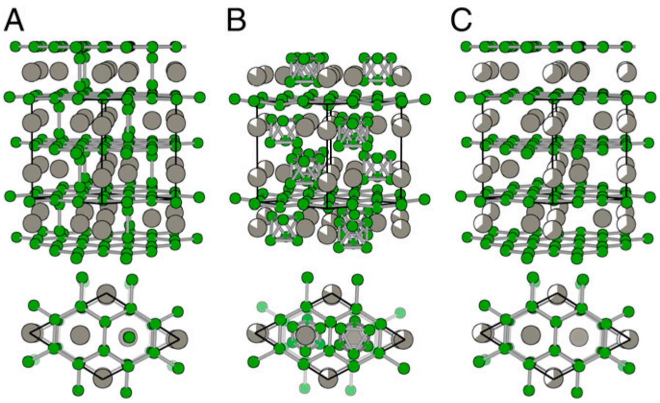

Fig. 2. Comparison of the various proposed structures of WB_4. (*A*) The structure of WB_4 by Romans and Krug (15). (*B*) The structure of $W_{1.83}B_9$ according to Nowotny et al. (16). (*C*) The structure of "$W_{1-x}B_3$" following Rosenberg and Lundström (17) and Zeiringer et al. (14) Green spheres represent boron atoms and gray spheres represent tungsten atoms. Partial occupancy is indicated by partial sphere filling. Bonds are shown to clarify the spatial arrangement only.

grains are found throughout arc-melted ingots (Fig. 3*A*). Unfortunately, the extreme chemical inertness and mechanical robustness of crystalline boron precludes its separation from the tungsten phase, necessitating the simultaneous refinement of both. Furthermore, boron is strongly adhered even to the macroscopic crystallites (Fig. 3*B*), reducing the possibility of obtaining high quality single-crystal data, particularly in the case of neutron diffraction.

Although β-boron produces only trivial interference with the X-ray diffraction data, its presence poses a more formidable challenge for the analysis of the neutron data: its many intense peaks heavily overlap those of the tungsten phase. Moreover, the structure of β-boron is imprecisely known due to a large amount of structural disorder at the interstices between icosahedra (31–37). Accordingly, the neutron diffraction experiment produces an exceptionally complex pattern from strong diffraction of the secondary β-rhombohedral boron phase, necessitating its simultaneous refinement. Nevertheless, the structure of the β-rhombohedral boron phase was found to be satisfactorily modeled by a slight modification of the atomic coordinates proposed by Hoard et al. (35) (see *SI Appendix* for details).

The powder X-ray diffraction pattern of a crushed ingot of nominal composition WB_{12} made with isotopically enriched ^{11}B (i.e., $W^{11}B_{12}$), may be readily indexed against a hexagonal unit cell with dimensions $a = 5.2001$ Å and $c = 6.3388$ Å in the space groups $P62c$, $P63mc$, or $P6_3/mmc$. A few contaminating lines are noticeable and fully indexable against β-rhombohedral boron, as would be expected given the large molar excess of boron in the reaction mixture. Most of these lines, with the exceptions of those at 11.92° 2θ [$(102)_{boron}$], 16.19° 2θ [$(110)_{boron}$], 17.56° 2θ [$(104)_{boron}$], and 19.09° 2θ [$(201)_{boron}$], are of similar magnitude (<1%) to those of residual $Cu_{K\beta}$ radiation diffracted by the WB_x phase. Although we have found no evidence supporting the *P-3* trigonal structure proposed by Nowotny et al. (16), comparison of our X-ray diffractographs to reflections presented in their work indicates the probable misassignment of the highest intensity β-boron peak (observable in our data at 17.56° 2θ in Fig. 4*B*) to the tungsten boride pattern. Using our data, we can readily replicate this reduction in symmetry, thus accounting for the discrepancy.

Here, we have chosen the highest symmetry group, $P6_3/mmc$, in which there are three crystallographic positions [Wyckoff *2*(*b*), *2(c)*, and *2(d)*] that may be occupied by tungsten atoms. One of these positions [Wyckoff *2(d)*] is completely unoccupied, and thus one-third of the maximum possible tungsten atoms are systematically absent, leaving "voids" in the structure. Rietveld analysis against a model consisting only of tungsten atoms and a hexagonal net of boron yielded a fractional occupancy of ∼2/3 for the tungsten atom at Wyckoff *2*(*b*) at (0, 0, 1/4). The last remaining tungsten site, Wyckoff *2(c)*, is fully occupied at (1/3, 2/3, 1/4).

Among the previous work on this subject, the structure derived by Zeiringer et al. (and related to that proposed by Rosenberg and Lundström) from single crystal data is the most similar to ours. However, repeated attempts at refining this model, where only voids are left for the partially occupied tungsten site, against the neutron powder diffraction data made clear that it does not fully account for the observed peak intensities (Fig. 4*C*). Fourier difference maps (Fig. 4*D*) subsequently revealed significant diffraction density on Wyckoff *6(h)* at approximately (0.24, 0.12, 1/4) and (0.26, 0.13, 1/4). A boron atom inserted into either of these positions refined to (0.24, 0.12, 1/4) with an occupancy of ∼1/3. The resulting model thoroughly accounts for the observed X-ray and neutron diffraction intensities and is compatible with our own single crystal measurements. Intriguingly, Rosenberg and Lundström mentioned peaks in their own Fourier mapping corresponding to at least ∼17% boron occupancy of the Wyckoff *6(h)*, but the potential for occupancy at this position was not explored. One might speculate that conclusions similar to those presented here might be reached if data for $Mo_{1-x}B_3$ were to be further refined against a model having such sites occupied.

The structure resulting from our analysis, presented in Fig. 5 (crystallographic parameters listed in Table 2), implies a stoichiometry of approximately $WB_{4.2}$. From this solution, we may draw some structural conclusions that have not been previously reported. Specifically, we find that a trigonal cluster of boron randomly fills the crystallographic position around the partially occupied tungsten *2*(*b*) site. Due to the relative site occupancies of these atoms [2/3 at *2*(*b*) for W and 1/3 at *6*(*h*) for B], as well as the unrealistically short bond distance that would result if both were present simultaneously, it is best to consider them a singular unit that is never partially occupied, but always filled by either tungsten or the boron trimer. This arrangement, where the boron atoms are well within bonding distance to the hexagonal boron nets, gives rise to a subset of slightly distorted cuboctahedra, or portions thereof, distributed between tungsten planes. The average incidence of these random cuboctahedra can be calculated as approximately one for every three cellular units (two trimers per cell). The effective void space in this structure is thus much smaller than that anticipated in other models, and the presence of boron between layers has the potential to provide bonding between boron layers.

Isolated boron dimers, such as those in the practically canonical Romans and Krug structure (15), are a rare crystallographic entity for borides with M:B ratios greater than ∼3:2 or lesser than

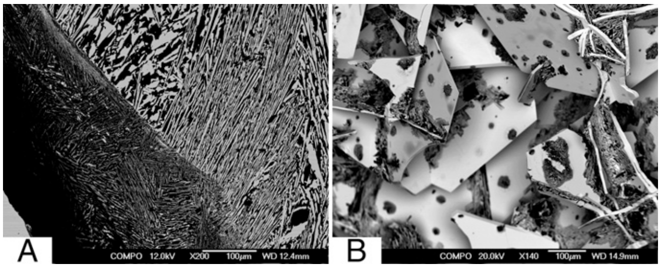

Fig. 3. (*A*) SEM image of a sectioned $W^{11}B_{12}$ ingot in backscattered electron (compositional) mode indicating compositional uniformity of $WB_{4.2}$ (bright) grains. (*B*) Backscattered electron SEM image of a fractured ingot of an arc-melted sample in the ratio W:B of 1:12. Light regions are the tungsten-containing phase.

CHEMISTRY

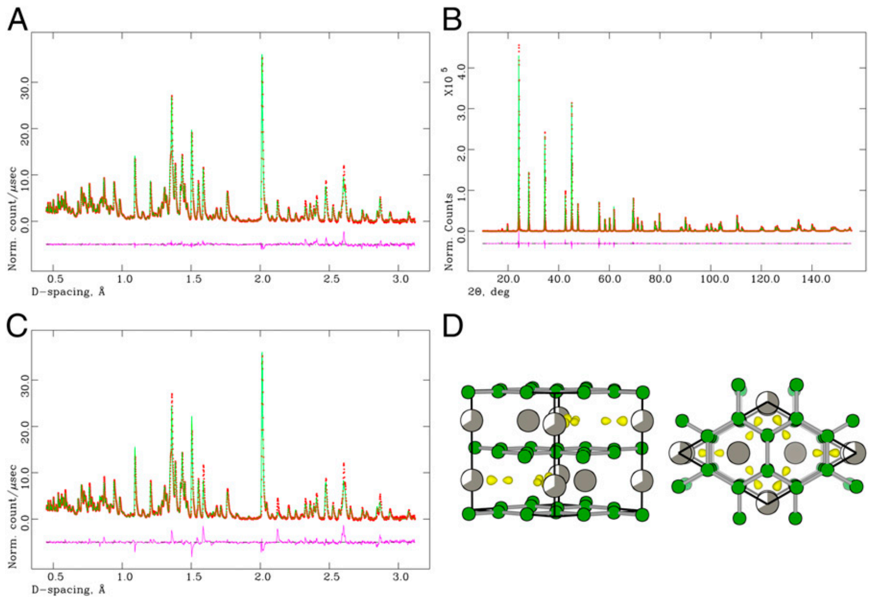

Fig. 4. (*A*) Neutron and (*B*) X-ray powder diffraction patterns for the highest boride of tungsten. Red points indicate observed data; the green line represents the fit against the final model. The difference between the two is shown beneath (magenta line). The background has been subtracted for clarity. (*C*) The best fit to the neutron diffraction data without the inclusion of the trigonal boron clusters. (*D*) Three-dimensional Fourier difference map (yellow) from the neutron refinement overlaid on the boron-deficient model structure lacking interstitial boron. Please see *SI Appendix* for enlarged plots.

~1:12, with few examples available in the literature. Their presence in this intermediate region contradicts the rule first described by Kiessling as early as 1951 (38)—that the structural connectivity of boron transitions from isolated atoms (e.g., W_2B) (39), to chains (e.g., WB) (39), to nets (e.g., WB_2) (39), to interconnected polyhedra (or portions thereof) as boron content increases. In fact, exceptions to this trend, such as the compound $IrB_{\sim1.35}$ (wherein apparent dimerization of boron is brought about by what can be imagined as a Peierls-type distortion of the boron chain) (40), often serve better to demonstrate the lawlikeness of Kiessling's rule than to contradict it. In those cases where isolated B_2 dimers do occur, such as for some borides of ratio M:B = 3:2 (e.g., W_2CoB_2) (41), they do so as a result of their intermediate stoichiometry between that of isolated-atom borides (M:B = 2:1) and chain-forming borides (M:B = 1:1). As such, they can be viewed as short chain fragments, with the trend continuing for M:B = 4:3, e.g., W_3CoB_3 (42) (three-atom chains), and so on.

Following that, the structure proposed here might itself be imagined as such an intermediate. For example, if all of the possible tungsten sites were to be fully occupied, an AlB_2-type (*P6*/*mmc*) structure with nearly ideal W–W and B–B distances would result. Conversely, if the absent tungsten sites are taken to give rise to the opportunistic formation of slightly distorted cuboctahedral cages, a hexagonal variation of the UB_{12}-type (*Fm-3m*) would be formed when all partially occupied tungsten sites are replaced (limiting stoichiometry = MB_9). This view is additionally satisfying in light of the stoichiometric position of $WB_{4.2}$ between MB_2-type compounds, which contain exclusively boron nets, and MB_x phases with $x > 2$, such as UB_{12}, where polyhedral subunits are increasingly dominant. The analogy can be further emphasized when a (somewhat fictionalized) representation of a tungsten boride having *all 6(h)* sites occupied is compared against the cubic packing of a scaled UB_{12} unit cell, as in Fig. 6. It can be rationalized that no higher tungsten boride having a "true" UB_{12} structure exists by noting that the formation of dodecaborides containing well-ordered cuboctahedra depends strongly on the radius of the metal atom, with Y (1.80 Å) (43) and Zr (1.60 Å) (43) being respectively, the largest and smallest metals to do so under ambient pressure (44). In comparison, the radius of W is only 1.39 Å (43), which is too small to accommodate one cuboctahedral cage per metal atom, as would be required. Notably, although, the second-neighbor M–M distances in $WB_{4.2}$ are ~5.200 Å, versus the nearest distance of ~5.236 Å for ZrB_{12} (45).

This model is further supported by data recently presented by Cheng et al. (20), who, using aberration corrected high-resolution transmission electron microscopy, claim to have visualized "interstitial boron" in WB_4. Nevertheless, the authors hypothesized that the true formula for the compound is WB_3, a composition they arrived at using particle swarm computational methods. In light of the microscopic evidence, they were forced to modify this formula to WB_{3+x} ($x \sim 0.343$–0.375) and further showed that this composition is compatible with their $2 \times 2 \times 2$ supercell. We speculate that, had the authors combined this information further and provided a crystallographic position for their interstitial boron, they may have found that full occupancy for both tungsten and boron in the sites they visualized is mutually exclusive. Indeed,

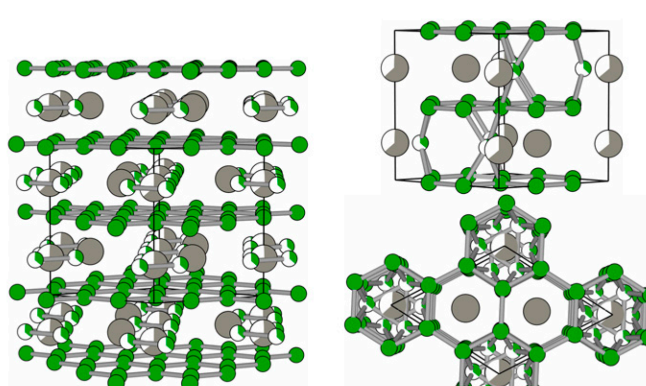

Fig. 5. The proposed structure of the highest boride of tungsten.

assuming the interstitial boron to be a crystallographic feature would have allowed for refinement against the X-ray diffraction data reported in their work, where the partial occupancy at tungsten *2*(*b*) becomes especially apparent. Had this last piece of information been included in their formula, it would have become $W_{0.833}B_{3.34} - W_{0.833}B_{3.375} = WB_{4.01} - WB_{4.05}$, which is close to the value of $WB_{4.2}$ reported here.

Finally, it is hoped that the model presented here might serve to unify the computational and experimental interpretations on this compound, as we do not find real contradiction between them. Indeed, although it is an experimental fact that one of the tungsten sites is partially occupied, it is simultaneously true that this same position is fully occupied, as this site is also the center of mass of the boron trimer that replaces it. In this way, the overall structure of the compound may be stable, even when calculations (without boron trimers) show fractional occupancy at tungsten *2(b)* to be unfavorable. Furthermore, we leave open the possibility of a range of stoichiometries for the highest boride of tungsten, and perhaps of other metals as well, all based on various degrees of polyhedral substitution at a metal site, with the formula derived here ($WB_{4.2}$) being only an end member. This observation may in fact turn out to be relatively common, and we might venture to propose that additional scrutiny of other nonstoichiometric borides with apparent homogeneity ranges above MB_2 could reveal similar phenomena. Indeed, there is already evidence of at least one other polyhedral replacement compound, where metal atoms are replaced instead by dimerically linked half-icosahedra, in the series $Mg_2M_{1-x}B_{6+2x}$ (M = Rh, Ir, $0.25 < x < 0.4$) of the Y_2ReB_6 structure type (46, 47).

Conclusions

In this work, we have presented a new crystal structure for the highest boride of tungsten, obtained by the simultaneous refinement of X-ray and neutron scattering data. The structure of this material has been debated for more than half a century, but the need for a definitive solution has increased dramatically in recent years with the discoveries that $WB_{4.2}$ is both superhard and can serve as the parent phase for a large family of solid solutions that are even harder (8, 9, 11). Although the crystal structure reported here contains some elements postulated previously—sites that are only partly occupied by tungsten, for example (14, 16, 17, 21)—the structure presents previously unidentified elements as well. The most important of these is the fact that the partially occupied tungsten sites that do not contain W atoms contain boron trimers, and these trimers are within the appropriate distance to couple with the boron layers, producing slightly distorted cuboctahedral boron cages. We postulate that this cage

Table 2. Relevant crystallographic data for the highest boride of tungsten

	W1	W2	B1	B2
Site	2c	2b	12i	6h
x	2/3	0	0.33167(11)	0.11887(11)
y	1/3	0	0	0.23775(23)
z	1/4	1/4	0	1/4
Occupancy	1	0.6412(6)	1	0.3569(11)
U_{iso}	0.00195	0.0013	0.00171	0.0044
U_{11}	0.00287(4)	0.00191(8)	0.001424(1)	0.00779(19)
U_{22}	0.00287(4)	0.00191(8)	0.001350(3)	0.00312(26)
U_{33}	0.00011(7)	0.00009(15)	0.002326(2)	0.00074(21)
U_{12}	0.001435(2)	0.00096(4)	0.000673(1)	0.00156(13)
U_{13}	0	0	0.00040(5)	0
U_{23}	0	0	0.00079(10)	0

Numbers in parentheses represent the uncertainty of the proceeding least significant figure.

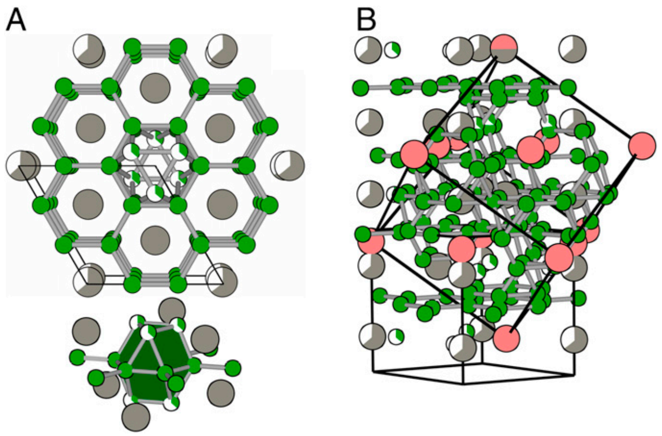

Fig. 6. (*A*) Occurrence of a cuboctahedron at the intersection of three unit cells. (*B*) Overlay of the UB_{12} structure type on $WB_{4.2}$, showing a close similarity.

structure is the primary bonding motif responsible for the remarkable hardness of $WB_{4.2}$.

We conclude by considering the implications of this new crystal structure to the hardness of $WB_{4.2}$. As mentioned above, $WB_{4.2}$ is capable of hosting a wide range of solute atoms, and these solute atoms can have a profound effect on hardness, even at very low concentrations (9). Having an accurate model for $WB_{4.2}$ provides valuable insight toward understanding these phenomena and more directly predicting the means of manipulating the crystal chemistry of this compound. For a low volume, high symmetry, binary compound, the unit cell of $WB_{4.2}$ contains an unusually large number of unique crystallographic sites. By carefully tailoring a solid solution scheme, it may be possible to select specific guest atoms to replace only the fully occupied tungsten site, only the partially occupied site, or both. It may further be possible to introduce other metals or heteroatoms at the vacant *2(d)* position, replacing the cuboctahedra with metal atoms or, conversely, enhancing the frequency and regularity with which they occur (9). Changes in the spatial distribution of boron cuboctahedra upon doping with metal heteroatoms could possibly be the basis for the extraordinary changes in hardness that can be achieved at doping levels of just a few percent. Perhaps most importantly, however, the existence of an accurate crystal structure for $WB_{4.2}$ should aid in the rational design of new superhard solid solutions using computational methods. As such, this previously unreported crystal structure has potential to lead to improvements in next generation superhard materials.

Materials and Methods

Samples for X-ray and neutron diffraction were prepared in parallel from the same batch of reagents and using the same methodology. High-purity powders of tungsten (99.95%; Strem Chemicals) and crystalline ^{11}B (99.9%, 98.2% ^{11}B enriched; Ceradyne) were manually mixed in the atomic ratio 1:12 using an agate mortar and pestle and consolidated into pellets by means of a hydraulic jack press (Carver). The pellets were placed on a water-cooled copper hearth inside a bell jar and purged several times with ultra-high-purity argon before being arc melted under ~100-A DC current from a nonconsumable tungsten cathode; ingots containing WB_4 platelets cool directly from the placental melt. The samples were crushed to powders using a hardened steel mortar and pestle (Humboldt) and wet ground under methanol/ethylene glycol at low speed in a planetary mill (Pulverisette 5/2; Fritsch) using stainless steel media until the majority passed through a 635 mesh (20 μm) screen (Humboldt). The sieved powders were stirred under three successive aliquots of excess HCl to remove residue from the grinding media. The submicron fraction of each sample was separated by repeated suspension in methanolic ammonia, the fastest settling fraction being retained. This procedure was found to minimize contamination to below the detection limit of the energy dispersive X-ray spectroscopic analyzer (EDAX; EDAX Inc.) mounted on our SEM (JEOL JSM 6700 F).

CHEMISTRY

Nanoindentation was performed using an MTS Nano Indenter XP (MTS) with a Berkovich diamond tip. After calibration of the indenter with a standard silica block, the samples were indented automatically overnight to a depth of 900 nm at 20 randomly determined points and the resulting load versus displacement plots were averaged. The nanoindentation hardness of the material was determined from the loading curves by the method of Oliver and Pharr (48).

Samples for powder X-ray diffraction were deposited directly from methanolic suspension onto silicon (511) "zero-background" plates. Excess sample was removed by a razor blade until nearly perfectly flat. Diffraction patterns were collected from 10° to 156° 2θ using an X'Pert Pro Bragg-Bentano geometry laboratory X-ray diffractometer (PANalytical), using nickel filtered $Cu_{K\alpha}$ radiation ($\lambda_{K\alpha1}$ = 1.540593 Å, $\lambda_{K\alpha2}$ = 1.5444274 Å) (49), rotating sample stage, 0.04 rad Soller slits, and X'Celerator position sensitive detector.

Neutron diffraction data were collected from the High-Pressure Preferred Orientation beam line at Los Alamos Neutron Science Center (LANCSE), Los Alamos National Lab, Los Alamos New Mexico. This is a neutron time-of-flight machine using five banks of ^{3}H-detector tube panels. Because of the extremely high thermal neutron absorption cross-section of residual ^{10}B, as well as that of natural W, this beam-line was selected due to its very high flux. Powdered samples ~1 cm^3 in volume were loaded into vanadium foil "cans" and irradiated by water-moderated neutrons collimated to 1 cm diameter, while data were collected for a cumulative collection time of 6 h. Powder X-ray and neutron diffraction data were subjected to simultaneous Rietveld refinement (50) using the EXPGUI (51) front-end to the GSAS (52) Rietveld refinement software package.

A single crystal of $WB_{4.2}$ containing natural boron was isolated from a crushed ingot obtained using the same arc-melting procedure described above. The crystal, having approximate dimensions 250 × 50 × 5 microns, was mounted on a loop filament on an APEX-II CCD diffractometer (Bruker). Using the Olex2 (53) structure solution program, the structure was solved by the charge flipping method and refined using Gauss–Newton minimization with eight parameters and without restraints.

ACKNOWLEDGMENTS. The authors thank Drs. Sven Vogel, Luke Deamon, and Helmut Reike at the Lujan Center of the Los Alamos National Laboratory for their help with neutron diffraction experiments; Dr. Saeed Khan for assistance with single-crystal X-ray diffractometry; and Professor Jeng-Ming Yang at the University of California, Los Angeles, Department of Materials Science and Engineering for use of his nanoindentation instrumentation. Ceradyne generously provided materials support through their provision of isotopically enriched ^{11}B, which we gratefully acknowledge. This research was supported financially by the National Science Foundation under Grant 1106364 (to S.H.T. and R.B.K.), the University of California Proof of Concept Program, and the Department of Energy under LANSCE Grant 20112198. Crystal-chemical illustrations in this work were made using the software package VESTA (54).

1. Cumberland RW, et al. (2005) Osmium diboride, an ultra-incompressible, hard material. *J Am Chem Soc* 127(20):7264–7265.
2. Chung H-Y, et al. (2007) Synthesis of ultra-incompressible superhard rhenium diboride at ambient pressure. *Science* 316(5823):436–439.
3. Kaner RB, Gilman JJ, Tolbert SH (2005) Materials science. Designing superhard materials. *Science* 308(5726):1268–1269.
4. Levine JB, Tolbert SH, Kaner RB (2009) Advancements in the search for superhard ultra-incompressible metal borides. *Adv Funct Mater* 19(22):3519–3533.
5. Komanduri R, Shaw MC (1975) Wear of synthetic diamond when grinding ferrous metals. *Nature* 255(5505):211–213.
6. Cook M, Bossom P (2000) Trends and recent developments in the material manufacture and cutting tool application of polycrystalline diamond and polycrystalline cubic boron nitride. *Int J Refract Met Hard Mater* 18(2-3):147–152.
7. Brazhkin VV, Lyapin AG, Hemley RJ (2002) Harder than diamond: Dreams and reality. *Philos Mag A* 82(2):231–253.
8. Mohammadi R, et al. (2011) Tungsten tetraboride, an inexpensive superhard material. *Proc Natl Acad Sci USA* 108(27):10958–10962.
9. Mohammadi R, et al. (2012) Toward inexpensive superhard materials: Tungsten tetraboride-based solid solutions. *J Am Chem Soc* 134(51):20660–20668.
10. Xie M, et al. (2012) Exploring the high-pressure behavior of superhard tungsten tetraboride. *Phys Rev B* 85(6):64118.
11. Gu Q, Krauss G, Steurer W (2008) Transition metal borides: Superhard versus ultra-incompressible. *Adv Mater* 20(19):3620–3626.
12. Xie M, et al. (2014) Lattice stress states of superhard tungsten tetraboride from radial x-ray diffraction under nonhydrostatic compression. *Phys Rev B* 90(10):104104.
13. Chretien A, Helgorsky J (1961) On new boride compositions of molybdenum and tungsten, MoB_4 and WB_4. *CR (East Lansing, Mich)* 252(5):742–744.
14. Zeiringer I, et al. (2014) Crystal structure of $W_{1-x}B_3$ and phase equilibria in the boron-rich part of the systems Mo-Rh-B and W-{Ru,Os,Rh,Ir,Ni,Pd,Pt}-B. *J Phase Equilibria Diffus.*
15. Romans Pa, Krug MP (1966) Composition and crystallographic data for the highest boride of tungsten. *Acta Crystallogr* 20(2):313–315.
16. Nowotny H, Haschke H, Benesovsky F (1967) Bor-reiche Wolframboride [Boron-rich tungsten borides]. *Monatsh Chem* 98(3):547–554. German.
17. Rosenberg I, Lundström T (1973) The crystal structure of the molybdenum boride $Mo_{1-x}B_3$. *J Solid State Chem* 6(2):299–305.
18. Liang Y, Gou Y, Yuan X, Zhong Z, Zhang W (2013) Unexpectedly hard and highly stable WB_3 with a noncompact structure. *Chem Phys Lett* 580(0):48–52.
19. Zang C, Sun H, Chen C (2012) Unexpectedly low indentation strength of WB_3 and MoB_3 from first principles. *Phys Rev B* 86(18):180101.
20. Cheng X, et al. (2013) Interstitial-boron solution strengthened WB_{3+x}. *Appl Phys Lett* 103(17):171903.
21. Gou H, Li Z, Wang L, Lian J, Wang Y (2012) Peculiar structure and tensile strength of WB_4: nonstoichiometric origin. *AIP Adv* 2(1):12171.
22. Zhang RF, et al. (2012) Stability and strength of transition-metal tetraborides and triborides. *Phys Rev Lett* 108(25):255502.
23. Liang Y, et al. (2012) An unexpected softening from WB_3 to WB_4. *Europhys Lett* 98(6):66004.
24. Wang M, Li Y, Cui T, Ma Y, Zou G (2008) Origin of hardness in WB_4 and its implications for ReB_4, TaB_4, MoB_4, TcB_4, and OsB_4. *Appl Phys Lett* 93(10):101905.
25. Zhang M, Yan H, Wei Q, Wang H (2013) Universal ground state hexagonal phases and mechanical properties of stoichiometric transition metal tetraborides: TMB_4 (TM=W, Tc, and Re). *Comput Mater Sci* 68(0):371–378.
26. Zhao E, Meng J, Ma Y, Wu Z (2010) Phase stability and mechanical properties of tungsten borides from first principles calculations. *Phys Chem Chem Phys* 12(40):13158–13165.
27. Liang Y, Yuan X, Zhang W (2011) Thermodynamic identification of tungsten borides. *Phys Rev B* 83(22):220102.
28. Liang Y, et al. (2014) Polytypism in superhard transition-metal triborides. *Sci Rep* 4:5063.
29. Cheng X-Y, Chen X-Q, Li D-Z, Li Y-Y (2014) Computational materials discovery: The case of the W-B system. *Acta Crystallogr Sect C Struct Chem* 70(Pt 2):85–103.
30. Nakayama T, Kim HK, Shimizu J, Kimura K (2008) Effects of metal doping on thermoelectric properties of arc-melted and hot-pressed-rhombohedral boron. *Mater Trans* 49(3):593–599.
31. Bullett DW (1986) Electronic structure studies of boron and boron-rich borides. *Boron-rich solids*, eds Emin D, Aselage T, Beckel CL, Howard IA, Wood C (AIP Publishing, Melville, NY), 140(1):249–259.
32. Bullett DW (1991) The electronic origin disorder in boron and boron-rich borides. *Boron-rich solids* (AIP Publishing, Melville, NY), 231(1):21–28.
33. Albert B, Hillebrecht H (2009) Boron: Elementary challenge for experimenters and theoreticians. *Angew Chem Int Ed Engl* 48(46):8640–8668.
34. Widom M, Mihalkovič M (2008) Symmetry-broken crystal structure of elemental boron at low temperature. *Phys Rev B* 77(6):064113.
35. Hoard JL, Sullenger DB, Kennard CHL, Hughes RE (1970) The structure analysis of β-rhombohedral boron. *J Solid State Chem* 1(2):268–277.
36. Werheit H, et al. (2012) Isotopic phonon effects in β-rhombohedral boron—Non-statistical isotope distribution. *J Phys Condens Matter* 24(17):175401.
37. Favia P, Stoto T, Carrard M, Stadelmann P-A, Zuppiroli L (1996) Order and disorder in boron phases. *Microsc Microanal Microstruct* 7(4):225–234.
38. Kiessling R (1951) The borides of some transition elements. *J Electrochem Soc* 98(4):166–170.
39. Okada S, Kudou K, Lundström T (1995) Preparations and some properties of W_2B, δ-WB and WB_2 crystals from high-temperature metal solutions. *Jpn J Appl Phys* 34(1):226–231.
40. Lundström T, et al. (1973) Refinement of the crystal structure of the non-stoichiometric boride $IrB_{\sim1.35}$. *Acta Chem Scand* 27(10):3705–3711.
41. Rieger W, Nowotny H, Benesovsky F (1966) [Die Kristallstruktur von W_2CoB_2 und isotypen Phasen]. *Monatsh Chem* 97(2):378–382. German.
42. Jedlicka H, Benesovsky F, Nowotny H (1969) [Die Kristallstruktur des W_3CoB_3 und der dazu isotypen Phasen Mo_3CoB_3, Mo_3NiB_3 und W_3NiB_3]. *Monatsh Chem* 100(3):844–850. German.
43. Pauling L (1947) Atomic radii and interatomic distances in metals. *J Am Chem Soc* 69(3):542–553.
44. La Placa S, Binder I, Post B (1961) Binary dodecaborides. *J Inorg Nucl Chem* 18(0):113–117.
45. Kennard CHL, Davis L (1983) Zirconium dodecarborides ZrB_{12}. Confirmation of the B_{12} cubooctahedral unit. *J Solid State Chem* 47(1):103–106.
46. Alekseeva AM, et al. (2007) Ternary magnesium rhodium boride $Mg_2Rh_{1-x}B_{6+2x}$ with a modified Y_2ReB_6-type crystal structure. *Inorg Chem* 46(18):7378–7386.
47. Alekseeva AM, et al. (2009) Crystal structure of magnesium iridium boride, $Mg_2Ir_{1-x}B_{6+2x}$ (x= 0.3). *Zeitschrift Krist* 224:19–20.
48. Oliver WC, Pharr GM (2011) An improved technique for determining hardness and elastic modulus using load and displacement sensing indentation experiments. *J Mater Res* 7(6):1564–1583.
49. Hölzer G, Fritsch M, Deutsch M, Härtwig J, Förster E (1997) $K_{\alpha\{1,2\}}$ and $K_{\beta\{1,3\}}$ x-ray emission lines of the 3d transition metals. *Phys Rev A* 56(6):4554–4568.
50. Rietveld HM (1969) A profile refinement method for nuclear and magnetic structures. *J Appl Cryst* 2(2):65–71.
51. Toby BH (2001) EXPGUI, A graphical user interface for GSAS. *J Appl Cryst* 34(2):210–213.
52. Larson AC, Von Dreele RB (2000) General Structure Analysis System (GSAS). *Los Alamos Natl Lab Rep* (LAUR 86-748).
53. Dolomanov OV, Bourhis LJ, Gildea RJ, Howard JAK, Puschmann H (2009) OLEX2: A complete structure solution, refinement and analysis program. *J Appl Cryst* 42(2):339–341.
54. Momma K, Izumi F (2008) VESTA: A three-dimensional visualization system for electronic and structural analysis. *J Appl Cryst* 41(3):653–658.